EUROPEAN ORGANIZATION FOR NUCLEAR RESEARCH

CERN-PH-EP/2004-005
March 3, 2004

Measurement of Exclusive $\rho^+\rho^-$ Production in High-Q^2 Two-Photon Collisions at LEP

The L3 Collaboration

Abstract

Exclusive $\rho^+\rho^-$ production in two-photon collisions involving a single highly-virtual photon is studied for the first time with data collected by the L3 experiment at LEP at centre-of-mass energies 89 GeV $< \sqrt{s} <$ 209 GeV with a total integrated luminosity of 854.7 pb^{-1}. The cross section of the process $\gamma\gamma^* \to \rho^+\rho^-$ is determined as a function of the photon virtuality, Q^2, and the two-photon centre-of-mass energy, $W_{\gamma\gamma}$, in the kinematic region: 1.2 GeV^2 $< Q^2 <$ 30 GeV^2 and 1.1 GeV $< W_{\gamma\gamma} <$ 3 GeV. The $\rho^+\rho^-$ production cross section is found to be of the same magnitude as the cross section of the process $\gamma\gamma^* \to \rho^0\rho^0$, measured in the same kinematic region by L3, and to have similar $W_{\gamma\gamma}$ and Q^2 dependences.

Submitted to *Phys. Lett. B*

1 Introduction

In this Letter, we present the first measurement of the process:

$$e^+e^- \to e^+e^-\gamma\gamma^* \to e^+e^-\rho^+\rho^- \tag{1}$$

in a kinematic region of large momentum transfer, obtained with data collected by the L3 detector [1] at LEP. In this kinematic domain, one of the interacting photons, γ, is quasi-real and the other, γ^*, has a large virtuality, Q^2, defined by a scattered electron[1)] detected ("tagged") in the forward electromagnetic calorimeter, used to measure the luminosity. This work continues our study of exclusive $\gamma\gamma^* \to \rho\rho$ production: our measurement of the process $\gamma\gamma^* \to \rho^0\rho^0$ was recently published [2] and here the charge-conjugate channel is analysed. The $\gamma\gamma \to \rho^+\rho^-$ exclusive production was previously studied only at low Q^2 for quasi-real photons [3, 4].

The interest in exclusive production of hadron pairs in two-photon interactions at high momentum transfer is due to recently developed methods for calculating the cross section of such processes in the framework of perturbative QCD [5]. In these models, the exclusive process is factorised into a perturbative, calculable, short-distance scattering $\gamma\gamma^* \to q\bar{q}$ or $\gamma\gamma^* \to gg$ and non-perturbative matrix elements describing the transition of the two partons into hadron pairs, which are called generalised distribution amplitudes. A comprehensive theoretical analysis of our $\gamma\gamma \to \rho^0\rho^0$ data [2] in this framework was recently performed [6].

The squared four-momentum transfer, Q^2, is determined by the beam energy, E_b, and the energy and scattering angle of the tagged electron, E_s and θ_s, by the relation:

$$Q^2 = 2E_bE_s(1 - \cos\theta_s). \tag{2}$$

The bremsstrahlung production of $\rho^+\rho^-$ pairs, which represents a background to the process (1), is strongly suppressed in the kinematic region of our measurement [7, 8].

The data used in this study, the kinematic regions covered and the analysis techniques employed are similar to those of our measurement of $\rho^0\rho^0$ production in tagged two-photon interactions [2]. The data correspond to an integrated luminosity of 854.7 pb^{-1}, out of which 148.7 pb^{-1} were collected at e^+e^- centre-of-mass energies, $\sqrt{s}$, around the Z resonance (Z pole), and 706.0 pb^{-1} at 161 GeV $\leq \sqrt{s} <$ 209 GeV (high energy), corresponding to an average $\sqrt{s}$ of 195 GeV. The production cross section is determined as a function of the invariant mass of the hadronic system, $W_{\gamma\gamma}$, and as a function of Q^2 in the kinematic region defined by the intervals:

$$1.2 \text{ GeV}^2 < Q^2 < 8.5 \text{ GeV}^2 \quad \text{(Z pole)}; \tag{3}$$

$$8.8 \text{ GeV}^2 < Q^2 < 30 \text{ GeV}^2 \quad \text{(high energy)}; \tag{4}$$

$$1.1 \text{ GeV} < W_{\gamma\gamma} < 3 \text{ GeV}. \tag{5}$$

The results are compared to our measurement of $\rho^0\rho^0$ production at high Q^2 and to the Vector Dominance model [9], as well as to the expectations of a QCD model [7].

2 Experimental considerations

The L3 detector is described in detail in Reference 10. The sub-detectors used for the study of the reaction (1) are the charged-particle tracker, the electromagnetic calorimeter and the

[1)] Throughout this Letter, the term "electron" denotes both electrons and positrons.

small-angle luminosity monitor. For this analysis, their fiducial volumes and thresholds are chosen so as to achieve the necessary resolution and background rejection, as discussed in the following.

The central detector is a cylindrical high resolution drift chamber, complemented by a silicon micro-vertex detector near the beam pipe, in a magnetic field of 0.5 T. A polar-angle fiducial volume is chosen as $15^\circ \leq \theta \leq 165^\circ$. The transverse momentum resolution is parametrised as $\sigma_{p_t}/p_t = 0.018\ p_t(\mathrm{GeV}) \oplus 0.02$. Only tracks which come from the interaction vertex, have transverse momentum greater than 100 MeV and an energy loss in the tracking chamber compatible with the pion hypothesis are considered in this analysis.

The electromagnetic calorimeter consists of an array of 10734 BGO crystals, with the form of a truncated pyramid of 2×2 cm^2 base. The crystals are arranged in two half barrels with a polar angle coverage $42^\circ \leq \theta \leq 138^\circ$ and in two end-caps covering $11.6^\circ \leq \theta \leq 38^\circ$ and $142^\circ \leq \theta \leq 168.4^\circ$. The material preceding the barrel part of the electromagnetic calorimeter, amounts to 20% of a radiation length, increasing to 60% of a radiation length in the endcap regions. The energy resolution, $\sigma_\mathrm{E}/\mathrm{E}$, varies from 5% at 50 MeV to about 1% for energies greater than 10 GeV. In the following, only showers with energy greater than 60 MeV are considered for π^0 reconstruction.

The luminosity monitor, installed on each side of the detector and also made out of BGO crystals, covers the polar angle range 25 mrad $\leq \theta \leq$ 68 mrad for the Z-pole runs and 31 mrad $\leq \theta \leq$ 65 mrad for the high-energy runs, when a mask was introduced to protect the detector from the beam halo.

3 Event selection

The reaction (1), contributing to the process

$$\mathrm{e^+e^-} \to \mathrm{e^+e^-_{tag}}\pi^+\pi^-\pi^0\pi^0, \tag{6}$$

is identified by a scattered beam electron, $\mathrm{e_{tag}}$, detected in the luminosity monitor, two charged pions measured in the tracking chamber, and energy clusters from the two-photon decays of the π^0's deposited in the electromagnetic calorimeter. These events are accepted by several independent triggers with major contributions coming from a charged-particle trigger [11], with different features for the Z-pole and high-energy data-taking periods, and an energy trigger demanding a large energy deposition in the luminosity monitor in coincidence with at least one track [12]. The combined trigger efficiency, as determined from the data itself, is $(85.2 \pm 3.8)\%$ at the Z pole and $(96.8 \pm 1.5)\%$ at high energy.

Single-tagged events are selected by requiring an electromagnetic cluster with energy greater then 80% of the beam energy reconstructed in the luminosity monitor.

The event candidates must have exactly two tracks with zero total charge and four or five photons, identified as isolated clusters in the electromagnetic calorimeter, not matched with a charged track. Photons are paired to reconstruct neutral pions and their effective mass must be between 100 MeV and 170 MeV, as shown in Figure 1a. To improve the resolution of the reconstructed π^0 four-momentum, a constrained 1C kinematic fit to the nominal π^0 mass is performed for each π^0 candidate. If more than one $\pi^0\pi^0$ combination exists in an event, the one with smallest sum of the χ^2 from the constrained fits of its constituent π^0's is taken. Events which contain an additional photon candidate, not used in the selected $\pi^0\pi^0$ pair, are retained only if the energy of that photon is less than 300 MeV and does not exceed

10% of the energy of the selected $\pi^0\pi^0$ combination. Allowing for these additional soft photon increases the acceptance. These "noise" photons are due to instrumental sources, to beam-related backgrounds or remnants of hadronic showers.

To ensure that an exclusive final state is detected, the momenta of the tagged electron and the four-pion system must be well balanced in the plane transverse to the beam direction. The total transverse momentum squared, p_t^2, of the four-pion final state and the scattered electron, shown in Figure 1b, is required to be less than 0.25 GeV^2.

Figure 1c shows the mass spectrum of the $\pi^+\pi^-\pi^0$ subsystem of the four-pion final state. Apart from an η signal near the kinematic threshold, no other resonance structure is visible. Final states containing η's represent a background to the process (1) and are removed by requiring the three-pion mass to be above 0.65 GeV.

After all cuts, 343 events are observed, out of which 224 events are at the Z pole and 119 events are at high energy. The four-pion mass spectrum of these events is shown in Figure 2a. The mass distribution of the $\pi^\pm\pi^0$ combinations of the selected events, shown in Figure 2b, shows a peak at the ρ mass. A clustering of entries is observed at the crossing of the $\rho^\pm$ mass bands in the correlation plot of the masses of the charged $\pi^\pm\pi^0$ combinations, shown in Figure 2c. No resonance structure is observed in Figure 2d for the correlation plot of the masses of the $\pi^+\pi^-$ and $\pi^0\pi^0$ combinations. These features of the two-particle mass correlations give evidence for a signal from $\rho^+\rho^-$ intermediate states.

4 Background estimation

The contribution to the selected sample due to e^+e^- annihilation is negligible. The background from tagged exclusive $\pi^+\pi^-\pi^0$ final states, where photon candidates due to noise mimic the second π^0, is also negligible, as found by studying the p_t^2 distribution of $e_{tag}\pi^+\pi^-\pi^0$ subsystems of the selected events.

Two sources of background remain: partially reconstructed events with higher particle multiplicities where tracks or photons escape detection and signal events with one or more photons substituted by photon candidates due to noise. The latter has a component of its p_t^2 distribution similar to that of the signal. These backgrounds are studied directly with the data.

To estimate the background due to feed-down from higher-multiplicity final states, we select data samples of the type $\pi^\pm\pi^\pm\pi^0\pi^0$. In addition, we select $\pi^+\pi^-\pi^0\pi^0\pi^0$ events and exclude one π^0 from the reconstruction.

An event-mixing technique is employed in order to reproduce events from the second background source: one or two photons forming a π^0 are excluded from a selected event and replaced by photons from another data event.

All these events are required to pass the event selection procedure discussed above, with the exception of the charge-conservation requirement for the $\pi^\pm\pi^\pm\pi^0\pi^0$ sample. For the $\pi^+\pi^-\pi^0\pi^0\pi^0$ events only the $\pi^+\pi^-\pi^0\pi^0$ subsystem is considered. The p_t^2 distributions of the accepted background-like data events are combined with the distribution of selected $\pi^+\pi^-\pi^0\pi^0$ Monte Carlo events so as to reproduce the measured p_t^2 distribution of the selected data events, as shown in Figure 1b. The contribution of the background from partially reconstructed events is on average three times higher than the second background. The result of this procedure, applied for the events in the kinematic region defined by the conditions (3), (4) and (5), is shown in Figure 1b and the background levels are quoted in Tables 1–3.

To estimate the uncertainties on the background correction, the background evaluation procedure is repeated by excluding, in turn, each of the background-like data samples. The larger

value between the statistical uncertainty on the background determination and the observed variation in the background levels is retained as uncertainty. It varies in the range $4\% - 8\%$.

5 Data analysis

The $\rho^+\rho^-$ production is studied in bins of Q^2 and $W_{\gamma\gamma}$. These variables are reconstructed with a resolution better than 3% and the chosen bin widths are such that the event migration between adjacent bins is negligible. The production cross section is determined in the restricted $W_{\gamma\gamma}$-region (5), which contains 287 events, of which 195 events are at the Z pole and 92 events are at high energy.

5.1 Production model

To estimate the number of $\rho^+\rho^-$ events in the selected four-pion data sample, we consider non-interfering contributions from three processes:

$$\begin{aligned} &\gamma\gamma^* \to \rho^+\rho^-; \\ &\gamma\gamma^* \to \rho^\pm\pi^\mp\pi^0; \\ &\gamma\gamma^* \to \pi^+\pi^-\pi^0\pi^0, \text{ non} - \text{resonant}. \end{aligned} \tag{7}$$

Our data do not show any evidence for sub-processes involving production of high-mass resonances. However, the $\rho^\pm\pi^\mp\pi^0$ term can absorb possible contributions from intermediate states containing $a_1(1260)$ and $a_2(1320)$ resonances.

Monte Carlo samples of the processes (7) are generated with the EGPC [13] program. About 6 million events of each sub-process are produced for both the Z-pole and the high-energy regions. The $W_{\gamma\gamma}$ and Q^2 dependences are those of the $\gamma\gamma$ luminosity function [14] and only isotropic production and phase-space decays are included. These events are processed in the same way as the data, introducing specific detector inefficiencies for the different data taking periods. For acceptance calculations, the Monte Carlo events are assigned a Q^2-dependent weight, evaluated using the GVDM [15] form-factor for both photons. The detection efficiencies, calculated taking into account the detector acceptance and the efficiency of the selection procedure, are listed in Tables 1–3. They are in the range of $3\% - 6\%$, very similar for all sub-processes. The efficiency is mostly limited by the kinematics of the two-photon reaction which boosts the hadronic system along the beam direction. The geometrical coverage of the electromagnetic-calorimeter fiducial-volume affects the photon acceptance and thus the efficiency for π^0 reconstruction.

The efficiency is found to be uniform in the two-photon centre-of-mass system and it is therefore insensitive to the details of the Monte Carlo production model. The angular distributions of the reconstructed Monte Carlo events are similar to the generator-level ones and in good agreement with those observed in data, as shown in Figure 3.

5.2 Fit method

The set, Ω, comprising the six two-pion masses in an event, namely the four charged combinations $\pi^\pm\pi^0$ and the two neutral combinations, $\pi^+\pi^-$ and $\pi^0\pi^0$, provides a complete description of a four-pion event in our model of isotropic production and decay. For each data event, i,

with measured variables Ω_i, we calculate the probabilities, $P_j(\Omega_i)$, that the event resulted from the production mechanism j. A likelihood function is defined as:

$$\Lambda = \prod_i \sum_{j=1}^{3} \lambda_j P_j(\Omega_i)\,, \qquad \sum_{j=1}^{3} \lambda_j = 1, \tag{8}$$

where λ_j is the fraction of the process j in the $\pi^+\pi^-\pi^0\pi^0$ sample for a given Q^2 or $W_{\gamma\gamma}$ bin and the product runs over all data events in that bin. The probabilities P_j are determined by the six-fold differential cross sections of the corresponding process, using Monte Carlo samples and a box method [16].

A maximum-likelihood fit reproduces the $\rho^+\rho^-$ content of Monte Carlo test samples within the statistical uncertainties. However, a large negative correlation exists between the $\rho^\pm\pi^\mp\pi^0$ and $\pi^+\pi^-\pi^0\pi^0$ (non-resonant) fitted fractions. Both contributions are necessary to fit the data. In the following, only the $\rho^+\rho^-$ content and the sum of the $\rho^\pm\pi^\mp\pi^0$ and $\pi^+\pi^-\pi^0\pi^0$ (non-resonant) contributions are considered.

To check the quality of the fit, the $\pi^\pm\pi^0$ mass distributions of the data are compared with those of a mixture of Monte Carlo event samples from the processes (7), in the proportion determined by the fit. The data and Monte Carlo distributions are in a good agreement over the entire Q^2 and $W_{\gamma\gamma}$ range, an example is shown in Figure 4. Figure 3 shows a similar comparison for some angular variables.

6 Results

The cross section, $\Delta\sigma_{\rm ee}$, of the process $\rm e^+e^- \to e^+e^-\rho^+\rho^-$ is measured as a function of Q^2 and $W_{\gamma\gamma}$. The results are listed in Tables 1–3, together with the efficiencies and the background fractions. The statistical uncertainties, listed in the Tables, are those of the fit. The differential cross section $d\sigma_{\rm ee}/dQ^2$, derived from $\Delta\sigma_{\rm ee}$, is listed in Table 1. When evaluating the differential cross section, a correction based on the Q^2-dependence of the $\rho^+\rho^-$ Monte Carlo sample is applied, so as to assign the cross section value to the centre of the corresponding Q^2-bin [17]. We also give in Table 1 the sum of the differential cross sections of the sub-processes leading to $\rho^\pm\pi^\mp\pi^0$ and $\pi^+\pi^-\pi^0\pi^0$ (non-resonant) final states.

To evaluate the cross section $\sigma_{\gamma\gamma}$ of the process $\gamma\gamma^* \to \rho^+\rho^-$, the integral of the transverse photon luminosity function, L_{TT}, is computed for each Q^2 and $W_{\gamma\gamma}$ bin using the program GALUGA [18], which performs $O(\alpha^4)$ QED calculations. The cross section $\sigma_{\gamma\gamma}$ is derived from the measured cross section $\Delta\sigma_{\rm ee}$ using the relation $\Delta\sigma_{\rm ee} = L_{TT}\sigma_{\gamma\gamma}$. Thus, $\sigma_{\gamma\gamma}$ represents an effective cross section containing contributions from both transverse and longitudinal photon polarisations. The cross sections of the process $\gamma\gamma^* \to \rho^+\rho^-$ are listed in Table 1 as a function of Q^2 and in Tables 2 and 3 as a function of $W_{\gamma\gamma}$. The sum of the cross sections of the processes $\gamma\gamma^* \to \rho^\pm\pi^\mp\pi^0$ and $\gamma\gamma^* \to \pi^+\pi^-\pi^0\pi^0$ (non-resonant) are also given in Tables 2 and 3.

To estimate the systematic uncertainties on the measured cross sections, we varied the selection of tracks and photons as well as the cuts in the event selection procedure, well beyond the resolution of the concerned variables. The contribution of the selection to the systematic uncertainties is in the range of $8\% - 18\%$. The contribution of the fitting procedure is estimated by varying the size and the occupancies of the boxes, as well as the binning of the data, and is found to be in the range of $10\% - 20\%$ for the fits in Q^2 bins and in the range of $10\% - 30\%$, for the fits in bins of $W_{\gamma\gamma}$. The systematic uncertainty of $4\% - 8\%$ introduced by the background correction procedure is also included. Different form-factor parameterisations were used for

re-weighting the Monte Carlo events and the observed variations of the acceptance correspond to a systematic uncertainty in the range of $2\% - 7\%$.

All contributions are added in quadrature to obtain the systematic uncertainties quoted in Tables 1–3. The overall normalisation uncertainties related to the trigger efficiency determination result in a 4% relative uncertainty between the Z-pole and high-energy data.

7 Discussion

The cross section of the process $\gamma\gamma^* \to \rho^+\rho^-$ as a function of $W_{\gamma\gamma}$ is plotted in Figure 5 together with the data from the L3 measurement of $\rho^0\rho^0$ production [2]. Both cross sections have similar dependence on $W_{\gamma\gamma}$ and are of the same magnitude, though the $\rho^+\rho^-$ cross section is systematically higher than the $\rho^0\rho^0$ one. The ratio of the cross section for $\rho^+\rho^-$ production relative to the $\rho^0\rho^0$ one, in the kinematic region 1.1 GeV $\leq W_{\gamma\gamma} \leq$ 2.1 GeV and 1.2 GeV$^2 \leq Q^2 \leq$ 8.5 GeV^2, is $\sigma(\rho^+\rho^-)/\sigma(\rho^0\rho^0) = 1.81 \pm 0.47\,(\text{stat.}) \pm 0.22\,(\text{syst.})$, compatible with the factor two expected for an isospin I = 0 state. These features of the $\rho\rho$ production at high Q^2 are in contrast with the different $W_{\gamma\gamma}$ dependence and the observed suppression by about a factor five of the $\rho^+\rho^-$ production with respect to $\rho^0\rho^0$ in the data for $Q^2 \approx 0$ and $W_{\gamma\gamma} < 2$ GeV [3, 4, 19]. A wide range of theoretical models was developed [20] to explain this feature, but the reason of this behaviour is still not understood [21]. The present measurement shows that this peculiarity disappears at high Q^2.

The cross section of the process $\gamma\gamma^* \to \rho^+\rho^-$ as a function of Q^2 is shown in Figure 6a, together with the L3 data for $\rho^0\rho^0$ production [2]. Both data sets have similar magnitude and Q^2 dependence. The $\rho^+\rho^-$ production cross section is fitted with a form-factor parametrisation [9] based on the generalised vector dominance model (GVDM) [15]. This is found to reproduce well the Q^2-dependence of the data, with a value of $\chi^2/\text{d.o.f.} = 1.31/4$.

Figure 6b shows the differential cross section $d\sigma_{\text{ee}}/dQ^2$ of the reaction $\text{e}^+\text{e}^- \to \text{e}^+\text{e}^-\rho^+\rho^-$, together with the L3 measurement for $\text{e}^+\text{e}^- \to \text{e}^+\text{e}^-\rho^0\rho^0$ [2]. As for $\rho^0\rho^0$ production, the $\rho^+\rho^-$ cross section is fitted to a form [8] expected from QCD-based calculations [7]:

$$\text{d}\sigma_{\text{ee}}/\text{d}Q^2 \sim \frac{1}{Q^n(Q^2 + < W_{\gamma\gamma} >^2)^2}\,, \tag{9}$$

with $< W_{\gamma\gamma} >= 1.91$ GeV being the average $W_{\gamma\gamma}$-value in the Q^2 intervals used. The fit provides a good description of the Q^2 dependence of the data, with $\chi^2/\text{d.o.f.} = 0.31/3$ and an exponent $n = 2.5 \pm 0.4$, to be compared with the expected value $n = 2$. Only statistical uncertainties are considered. A common fit of the data taken at the Z pole and at high energy is justified by the almost constant values of the photon polarisation parameter ϵ, which determines the energy dependence of the cross section. This result, together with that of our previous fit to $\rho^0\rho^0$ data, $n = 2.4 \pm 0.3$ [2], provides further evidence for similar Q^2 dependence of the $\rho^+\rho^-$ and $\rho^0\rho^0$ production in the kinematic region (3)–(5).

References

[1] L3 Coll., B. Adeva *et al.*, Nucl. Instr. Meth. A **289** (1990) 35; M. Chemarin *et al.*, Nucl. Instr. Meth. A **349** (1994) 345; M. Acciarri *et al.*, Nucl. Instr. Meth. A **351** (1994) 300; I.C. Brock *et al.*, Nucl. Instr. Meth. A **381** (1996) 236; A. Adam *et al.*, Nucl. Instr. Meth. A **383** (1996) 342.

[2] L3 Coll., P. Achard *et al.*, Phys. Lett. B **568** (2003) 11.

[3] ARGUS Coll., H. Albrecht *et al.*, Phys. Lett. B **217** (1989) 205; Phys. Lett. B **267** (1991) 535; Z. Phys. C **50** (1991) 1.

[4] CELLO Coll., H.-J. Behrend *et al.*, Z. Phys. C **21** (1984) 205; Phys. Lett. B **218** (1989) 493.

[5] M. Diehl, T. Gousset, B. Pire and O.V. Teryaev, Phys. Rev. Lett. **81** (1998) 1782; N. Kivel, L. Mankiewicz and M.V. Polyakov, Phys. Lett. B **467** (1999) 263; A. Freund, Phys. Rev. D **61** (2000) 074010.

[6] I.V. Anikin, B. Pire and O.V. Teryaev, Phys. Rev. D **69** (2004) 014018.

[7] M. Diehl, T. Gousset and B. Pire, Phys. Rev. D **62** (2000) 073014.

[8] M. Diehl private communication. We thank M. Diehl for very useful discussions.

[9] I.F. Ginzburg and V.G. Serbo, Phys. Lett. B **109** (1982) 231.

[10] L3 Coll., B. Adeva *et al.*, Nucl. Instr. Meth. A **289** (1990) 35.

[11] P. Béné *et al.*, Nucl. Instr. Meth. A **306** (1991) 150; D. Haas *et al.*, Nucl. Instr. Meth. A **420** (1999) 101.

[12] R. Bizzarri *et al.*, Nucl. Instr. Meth. A **283** (1989) 799.

[13] F.L. Linde, Ph.D. thesis, Rijksuniversiteit Leiden (1988).

[14] V.M. Budnev *et al.*, Phys. Rep. C **15** (1975) 181.

[15] J.J. Sakurai and D. Schildknecht, Phys. Lett. B **40** (1972) 121.

[16] D.M. Schmidt, R.J. Morrison and M.S. Witherell, Nucl. Instr. Meth. A **328** (1993) 547.

[17] G.D. Lafferty and T.R. Wyatt, Nucl. Instr. Meth. A **355** (1995) 541.

[18] G.A. Schuler, Comput. Phys. Commun. **108** (1998) 279.

[19] TASSO Coll., R. Brandelik *et al.*, Phys. Lett. B **97** (1980) 448; M. Althoff *et al.*, Z. Phys. C **16** (1982) 13; MARK II Coll., D.L. Burke *et al.*, Phys. Lett. B **103** (1981) 153; TPC/2γ Coll., H. Aihara *et al.*, Phys. Rev. D **37** (1988) 28; PLUTO Coll., Ch. Berger *et al.*, Z. Phys. C **38** (1988) 521.

[20] N.N. Achasov *et al.*, Phys. Lett. B **108** (1982) 134; Z. Phys. C **16** (1982) 55; Phys. Lett. B **203** (1988) 309; G. Alexander *et al.*, Phys. Rev. D **26** (1982) 1198; Z. Phys. C **30** (1986) 65; B.A. Li and K.F. Liu, Phys. Lett. B **118** (1982) 435; Phys. Lett. B **124** (1983) 550; Phys. Rev. D **30** (1984) 613; Phys. Rev. Lett. **58** (1987) 2288; S.J. Brodsky, G. Köpp and P.M. Zerwas, Phys. Rev. Lett. **58** (1987) 443.

[21] J.L. Rosner hep-ph/0404245 (2004), to be published in Phys. Rev. D.

The L3 Collaboration:

P.Achard,[20] O.Adriani,[17] M.Aguilar-Benitez,[25] J.Alcaraz,[25] G.Alemanni,[23] J.Allaby,[18] A.Aloisio,[29] M.G.Alviggi,[29] H.Anderhub,[49] V.P.Andreev,[6,34] F.Anselmo,[8] A.Arefiev,[28] T.Azemoon,[3] T.Aziz,[9] P.Bagnaia,[39] A.Bajo,[25] G.Baksay,[26] L.Baksay,[26] S.V.Baldew,[2] S.Banerjee,[9] Sw.Banerjee,[4] A.Barczyk,[49,47] R.Barillère,[18] P.Bartalini,[23] M.Basile,[8] N.Batalova,[46] R.Battiston,[33] A.Bay,[23] F.Becattini,[17] U.Becker,[13] F.Behner,[49] L.Bellucci,[17] R.Berbeco,[3] J.Berdugo,[25] P.Berges,[13] B.Bertucci,[33] B.L.Betev,[49] M.Biasini,[33] M.Biglietti,[29] A.Biland,[49] J.J.Blaising,[4] S.C.Blyth,[35] G.J.Bobbink,[2] A.Böhm,[1] L.Boldizsar,[12] B.Borgia,[39] S.Bottai,[17] D.Bourilkov,[49] M.Bourquin,[20] S.Braccini,[20] J.G.Branson,[41] F.Brochu,[4] J.D.Burger,[13] W.J.Burger,[33] X.D.Cai,[13] M.Capell,[13] G.Cara Romeo,[8] G.Carlino,[29] A.Cartacci,[17] J.Casaus,[25] F.Cavallari,[39] N.Cavallo,[36] C.Cecchi,[33] M.Cerrada,[25] M.Chamizo,[20] Y.H.Chang,[44] M.Chemarin,[24] A.Chen,[44] G.Chen,[7] G.M.Chen,[7] H.F.Chen,[22] H.S.Chen,[7] G.Chiefari,[29] L.Cifarelli,[40] F.Cindolo,[8] I.Clare,[13] R.Clare,[38] G.Coignet,[4] N.Colino,[25] S.Costantini,[39] B.de la Cruz,[25] S.Cucciarelli,[33] J.A.van Dalen,[31] R.de Asmundis,[29] P.Déglon,[20] J.Debreczeni,[12] A.Degré,[4] K.Dehmelt,[26] K.Deiters,[47] D.della Volpe,[29] E.Delmeire,[20] P.Denes,[37] F.DeNotaristefani,[39] A.De Salvo,[49] M.Diemoz,[39] M.Dierckxsens,[2] C.Dionisi,[39] M.Dittmar,[49] A.Doria,[29] M.T.Dova,[10,♯] D.Duchesneau,[4] M.Duda,[1] B.Echenard,[20] A.Eline,[18] A.El Hage,[1] H.El Mamouni,[24] A.Engler,[35] F.J.Eppling,[13] P.Extermann,[20] M.A.Falagan,[25] S.Falciano,[39] A.Favara,[32] J.Fay,[24] O.Fedin,[34] M.Felcini,[49] T.Ferguson,[35] H.Fesefeldt,[1] E.Fiandrini,[33] J.H.Field,[20] F.Filthaut,[31] P.H.Fisher,[13] W.Fisher,[37] I.Fisk,[41] G.Forconi,[13] K.Freudenreich,[49] C.Furetta,[27] Yu.Galaktionov,[28,13] S.N.Ganguli,[9] P.Garcia-Abia,[25] M.Gataullin,[32] S.Gentile,[39] S.Giagu,[39] Z.F.Gong,[22] G.Grenier,[24] O.Grimm,[49] M.W.Gruenewald,[16] M.Guida,[40] V.K.Gupta,[37] A.Gurtu,[9] L.J.Gutay,[46] D.Haas,[5] D.Hatzifotiadou,[8] T.Hebbeker,[1] A.Hervé,[18] J.Hirschfelder,[35] H.Hofer,[49] M.Hohlmann,[26] G.Holzner,[49] S.R.Hou,[44] Y.Hu,[31] B.N.Jin,[7] L.W.Jones,[3] P.de Jong,[2] I.Josa-Mutuberría,[25] M.Kaur,[14] M.N.Kienzle-Focacci,[20] J.K.Kim,[43] J.Kirkby,[18] W.Kittel,[31] A.Klimentov,[13,28] A.C.König,[31] M.Kopal,[46] V.Koutsenko,[13,28] M.Kräber,[49] R.W.Kraemer,[35] A.Krüger,[48] A.Kunin,[13] P.Ladron de Guevara,[25] I.Laktineh,[24] G.Landi,[17] M.Lebeau,[18] A.Lebedev,[13] P.Lebrun,[24] P.Lecomte,[49] P.Lecoq,[18] P.Le Coultre,[49] J.M.Le Goff,[18] R.Leiste,[48] M.Levtchenko,[27] P.Levtchenko,[34] C.Li,[22] S.Likhoded,[48] C.H.Lin,[44] W.T.Lin,[44] F.L.Linde,[2] L.Lista,[29] Z.A.Liu,[7] W.Lohmann,[48] E.Longo,[39] Y.S.Lu,[7] C.Luci,[39] L.Luminari,[39] W.Lustermann,[49] W.G.Ma,[22] L.Malgeri,[20] A.Malinin,[28] C.Maña,[25] J.Mans,[37] J.P.Martin,[24] F.Marzano,[39] K.Mazumdar,[9] R.R.McNeil,[6] S.Mele,[18,29] L.Merola,[29] M.Meschini,[17] W.J.Metzger,[31] A.Mihul,[11] H.Milcent,[18] G.Mirabelli,[39] J.Mnich,[1] G.B.Mohanty,[9] G.S.Muanza,[24] A.J.M.Muijs,[2] B.Musicar,[41] M.Musy,[39] S.Nagy,[15] S.Natale,[20] M.Napolitano,[29] F.Nessi-Tedaldi,[49] H.Newman,[32] A.Nisati,[39] T.Novak,[31] H.Nowak,[48] R.Ofierzynski,[49] G.Organtini,[39] I.Pal,[46] C.Palomares,[25] P.Paolucci,[29] R.Paramatti,[39] G.Passaleva,[17] S.Patricelli,[29] T.Paul,[10] M.Pauluzzi,[33] C.Paus,[13] F.Pauss,[49] M.Pedace,[39] S.Pensotti,[27] D.Perret-Gallix,[4] B.Petersen,[31] D.Piccolo,[29] F.Pierella,[8] M.Pioppi,[33] P.A.Piroué,[37] E.Pistolesi,[27] V.Plyaskin,[28] M.Pohl,[20] V.Pojidaev,[17] J.Pothier,[18] D.Prokofiev,[34] J.Quartieri,[40] G.Rahal-Callot,[49] M.A.Rahaman,[9] P.Raics,[15] N.Raja,[9] R.Ramelli,[49] P.G.Rancoita,[27] R.Ranieri,[17] A.Raspereza,[48] P.Razis,[30] D.Ren,[49] M.Rescigno,[39] S.Reucroft,[10] S.Riemann,[48] K.Riles,[3] B.P.Roe,[3] L.Romero,[25] A.Rosca,[48] C.Rosemann,[1] C.Rosenbleck,[1] S.Rosier-Lees,[4] S.Roth,[1] J.A.Rubio,[18] G.Ruggiero,[17] H.Rykaczewski,[49] A.Sakharov,[49] S.Saremi,[6] S.Sarkar,[39] J.Salicio,[18] E.Sanchez,[25] C.Schäfer,[18] V.Schegelsky,[34] H.Schopper,[21] D.J.Schotanus,[31] C.Sciacca,[29] L.Servoli,[33] S.Shevchenko,[32] N.Shivarov,[42] V.Shoutko,[13] E.Shumilov,[28] A.Shvorob,[32] D.Son,[43] C.Souga,[24] P.Spillantini,[17] M.Steuer,[13] D.P.Stickland,[37] B.Stoyanov,[42] A.Straessner,[20] K.Sudhakar,[9] G.Sultanov,[42] L.Z.Sun,[22] S.Sushkov,[1] H.Suter,[49] J.D.Swain,[10] Z.Szillasi,[26,¶] X.W.Tang,[7] P.Tarjan,[15] L.Tauscher,[5] L.Taylor,[10] B.Tellili,[24] D.Teyssier,[24] C.Timmermans,[31] Samuel C.C.Ting,[13] S.M.Ting,[13] S.C.Tonwar,[9] J.Tóth,[12] C.Tully,[37] K.L.Tung,[7] J.Ulbricht,[49] E.Valente,[39] R.T.Van de Walle,[31] R.Vasquez,[46] V.Veszpremi,[26] G.Vesztergombi,[12] I.Vetlitsky,[28] D.Vicinanza,[40] G.Viertel,[49] S.Villa,[38] M.Vivargent,[4] S.Vlachos,[5] I.Vodopianov,[26] H.Vogel,[35] H.Vogt,[48] I.Vorobiev,[35,28] A.A.Vorobyov,[34] M.Wadhwa,[5] Q.Wang,[31] X.L.Wang,[22] Z.M.Wang,[22] M.Weber,[18] H.Wilkens,[31] S.Wynhoff,[37] L.Xia,[32] Z.Z.Xu,[22] J.Yamamoto,[3] B.Z.Yang,[22] C.G.Yang,[7] H.J.Yang,[3] M.Yang,[7] S.C.Yeh,[45] An.Zalite,[34] Yu.Zalite,[34] Z.P.Zhang,[22] J.Zhao,[22] G.Y.Zhu,[7] R.Y.Zhu,[32] H.L.Zhuang,[7] A.Zichichi,[8,18,19] B.Zimmermann,[49] M.Zöller.[1]

1 III. Physikalisches Institut, RWTH, D-52056 Aachen, Germany§
2 National Institute for High Energy Physics, NIKHEF, and University of Amsterdam, NL-1009 DB Amsterdam, The Netherlands
3 University of Michigan, Ann Arbor, MI 48109, USA
4 Laboratoire d'Annecy-le-Vieux de Physique des Particules, LAPP,IN2P3-CNRS, BP 110, F-74941 Annecy-le-Vieux CEDEX, France
5 Institute of Physics, University of Basel, CH-4056 Basel, Switzerland
6 Louisiana State University, Baton Rouge, LA 70803, USA
7 Institute of High Energy Physics, IHEP, 100039 Beijing, China△
8 University of Bologna and INFN-Sezione di Bologna, I-40126 Bologna, Italy
9 Tata Institute of Fundamental Research, Mumbai (Bombay) 400 005, India
10 Northeastern University, Boston, MA 02115, USA
11 Institute of Atomic Physics and University of Bucharest, R-76900 Bucharest, Romania
12 Central Research Institute for Physics of the Hungarian Academy of Sciences, H-1525 Budapest 114, Hungary‡
13 Massachusetts Institute of Technology, Cambridge, MA 02139, USA
14 Panjab University, Chandigarh 160 014, India
15 KLTE-ATOMKI, H-4010 Debrecen, Hungary¶
16 Department of Experimental Physics, University College Dublin, Belfield, Dublin 4, Ireland
17 INFN Sezione di Firenze and University of Florence, I-50125 Florence, Italy
18 European Laboratory for Particle Physics, CERN, CH-1211 Geneva 23, Switzerland
19 World Laboratory, FBLJA Project, CH-1211 Geneva 23, Switzerland
20 University of Geneva, CH-1211 Geneva 4, Switzerland
21 University of Hamburg, D-22761 Hamburg, Germany
22 Chinese University of Science and Technology, USTC, Hefei, Anhui 230 029, China△
23 University of Lausanne, CH-1015 Lausanne, Switzerland
24 Institut de Physique Nucléaire de Lyon, IN2P3-CNRS,Université Claude Bernard, F-69622 Villeurbanne, France
25 Centro de Investigaciones Energéticas, Medioambientales y Tecnológicas, CIEMAT, E-28040 Madrid, Spain♭
26 Florida Institute of Technology, Melbourne, FL 32901, USA
27 INFN-Sezione di Milano, I-20133 Milan, Italy
28 Institute of Theoretical and Experimental Physics, ITEP, Moscow, Russia
29 INFN-Sezione di Napoli and University of Naples, I-80125 Naples, Italy
30 Department of Physics, University of Cyprus, Nicosia, Cyprus
31 University of Nijmegen and NIKHEF, NL-6525 ED Nijmegen, The Netherlands
32 California Institute of Technology, Pasadena, CA 91125, USA
33 INFN-Sezione di Perugia and Università Degli Studi di Perugia, I-06100 Perugia, Italy
34 Nuclear Physics Institute, St. Petersburg, Russia
35 Carnegie Mellon University, Pittsburgh, PA 15213, USA
36 INFN-Sezione di Napoli and University of Potenza, I-85100 Potenza, Italy
37 Princeton University, Princeton, NJ 08544, USA
38 University of Californa, Riverside, CA 92521, USA
39 INFN-Sezione di Roma and University of Rome, "La Sapienza", I-00185 Rome, Italy
40 University and INFN, Salerno, I-84100 Salerno, Italy
41 University of California, San Diego, CA 92093, USA
42 Bulgarian Academy of Sciences, Central Lab. of Mechatronics and Instrumentation, BU-1113 Sofia, Bulgaria
43 The Center for High Energy Physics, Kyungpook National University, 702-701 Taegu, Republic of Korea
44 National Central University, Chung-Li, Taiwan, China
45 Department of Physics, National Tsing Hua University, Taiwan, China
46 Purdue University, West Lafayette, IN 47907, USA
47 Paul Scherrer Institut, PSI, CH-5232 Villigen, Switzerland
48 DESY, D-15738 Zeuthen, Germany
49 Eidgenössische Technische Hochschule, ETH Zürich, CH-8093 Zürich, Switzerland
§ Supported by the German Bundesministerium für Bildung, Wissenschaft, Forschung und Technologie.
‡ Supported by the Hungarian OTKA fund under contract numbers T019181, F023259 and T037350.
¶ Also supported by the Hungarian OTKA fund under contract number T026178.
♭ Supported also by the Comisión Interministerial de Ciencia y Tecnología.
♯ Also supported by CONICET and Universidad Nacional de La Plata, CC 67, 1900 La Plata, Argentina.
△ Supported by the National Natural Science Foundation of China.

Q^2-range [GeV^2]	ε [%]	Bg [%]	$\Delta\sigma_{ee}$ [pb] $\rho^+\rho^-$	$d\,\sigma_{ee}/d\,Q^2$ [pb / GeV^2] $\rho^+\rho^-$	$\sigma_{\gamma\gamma}$ [nb] $\rho^+\rho^-$	$d\,\sigma_{ee}/d\,Q^2$ [pb / GeV^2] $\rho^\pm\pi^\mp\pi^0 + \pi^+\pi^-\pi^0\pi^0$
1.2 – 2.2	3.7	19	$6.30 \pm 1.63 \pm 1.07$	$6.06 \pm 1.57 \pm 1.03$	$5.12 \pm 1.32 \pm 0.87$	$8.63 \pm 1.71 \pm 1.21$
2.2 – 3.5	5.0	18	$2.57 \pm 0.96 \pm 0.58$	$1.85 \pm 0.69 \pm 0.41$	$3.33 \pm 1.24 \pm 0.75$	$3.51 \pm 0.80 \pm 0.54$
3.5 – 8.5	5.6	18	$2.11 \pm 0.81 \pm 0.41$	$0.31 \pm 0.12 \pm 0.06$	$1.98 \pm 0.77 \pm 0.38$	$0.53 \pm 0.13 \pm 0.07$
8.8 – 14.0	5.6	16	$0.38 \pm 0.135 \pm 0.072$	$0.067 \pm 0.024 \pm 0.013$	$0.74 \pm 0.26 \pm 0.14$	$0.14 \pm 0.029 \pm 0.019$
14.0 – 30.0	6.3	17	$0.23 \pm 0.099 \pm 0.060$	$0.011 \pm 0.0046 \pm 0.0029$	$0.40 \pm 0.17 \pm 0.10$	$0.024 \pm 0.0058 \pm 0.0041$

Table 1: Detection efficiencies, ε, background fractions, Bg, and measured production cross sections as a function of Q^2 for 1.1 GeV $< W_{\gamma\gamma} <$ 3 GeV for Z-pole and high-energy data. The first uncertainties are statistical, the second systematic. The values of the differential cross section are corrected to the centre of each bin.

$W_{\gamma\gamma}$-range [GeV]	ε [%]	Bg [%]	$\Delta\sigma_{ee}$ [pb] $\rho^+\rho^-$	$\sigma_{\gamma\gamma}$ [nb] $\rho^+\rho^-$	$\sigma_{\gamma\gamma}$ [nb] $\rho^\pm\pi^\mp\pi^0 + \pi^+\pi^-\pi^0\pi^0$
1.1 – 1.5	3.2	28	$3.09 \pm 1.18 \pm 0.96$	$3.99 \pm 1.53 \pm 1.24$	$7.51 \pm 1.78 \pm 1.43$
1.5 – 1.8	4.2	17	$3.67 \pm 1.04 \pm 0.55$	$6.84 \pm 1.93 \pm 1.03$	$7.90 \pm 2.03 \pm 1.15$
1.8 – 2.1	4.6	14	$2.79 \pm 0.81 \pm 0.39$	$5.62 \pm 1.63 \pm 0.79$	$6.57 \pm 1.74 \pm 0.88$
2.1 – 3.0	5.3	14	$1.95 \pm 0.69 \pm 0.38$	$1.55 \pm 0.55 \pm 0.30$	$3.87 \pm 0.74 \pm 0.50$

Table 2: Detection efficiencies, ε, background fractions, Bg, and measured production cross sections as a function of $W_{\gamma\gamma}$, for 1.2 GeV^2 $< Q^2 <$ 8.5 GeV^2, for the Z-pole data, together with the cross sections of the reactions $e^+e^- \to e^+e^-\rho^+\rho^-$, $\gamma\gamma^* \to \rho^+\rho^-$ and the sum of the cross sections of the processes $\gamma\gamma^* \to \rho^\pm\pi^\mp\pi^0$ and $\gamma\gamma^* \to \pi^+\pi^-\pi^0\pi^0$(non-resonant). The first uncertainties are statistical, the second systematic.

$W_{\gamma\gamma}$-range [GeV]	ε [%]	Bg [%]	$\Delta\sigma_{ee}$ [pb] $\rho^+\rho^-$	$\sigma_{\gamma\gamma}$ [nb] $\rho^+\rho^-$	$\sigma_{\gamma\gamma}$ [nb] $\rho^\pm\pi^\mp\pi^0 + \pi^+\pi^-\pi^0\pi^0$
1.1 – 1.7	4.9	24	$0.218 \pm 0.109 \pm 0.059$	$0.62 \pm 0.31 \pm 0.17$	$1.12 \pm 0.37 \pm 0.25$
1.7 – 2.2	6.1	16	$0.272 \pm 0.119 \pm 0.082$	$0.95 \pm 0.42 \pm 0.29$	$1.52 \pm 0.48 \pm 0.33$
2.2 – 3.0	6.4	11	$0.121 \pm 0.078 \pm 0.040$	$0.27 \pm 0.18 \pm 0.09$	$1.10 \pm 0.26 \pm 0.21$

Table 3: Detection efficiency, ε, background fractions, Bg, and measured production cross sections as a function of $W_{\gamma\gamma}$, for 8.8 GeV^2 $< Q^2 <$ 30 GeV^2, for the high energy data. together with the cross sections of the reactions $e^+e^- \to e^+e^-\rho^+\rho^-$, $\gamma\gamma^* \to \rho^+\rho^-$ and the sum of the cross sections of the processes $\gamma\gamma^* \to \rho^\pm\pi^\mp\pi^0$ and $\gamma\gamma^* \to \pi^+\pi^-\pi^0\pi^0$(non-resonant). The first uncertainties are statistical, the second systematic.

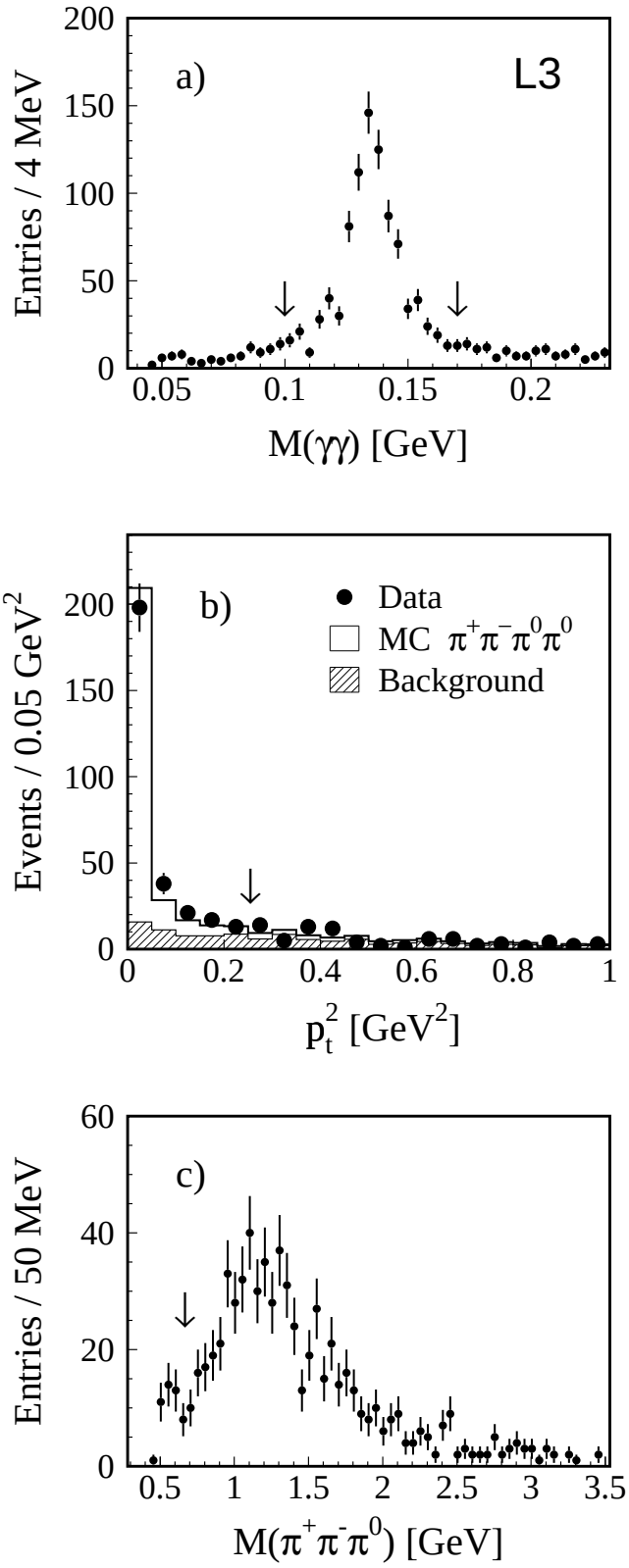

Figure 1: Observed distribution of a) the two-photon effective mass (two entries per event); b) the event p_t^2 for 1.1 GeV $< W_{\gamma\gamma} <$ 3 GeV; c) the mass of the $\pi^+\pi^-\pi^0$ system (two entries per event). Monte Carlo simulation of four-pion events (open histogram) and the background estimated from the data (hatched histogram) are also shown in b). The arrows indicate the selection cuts.

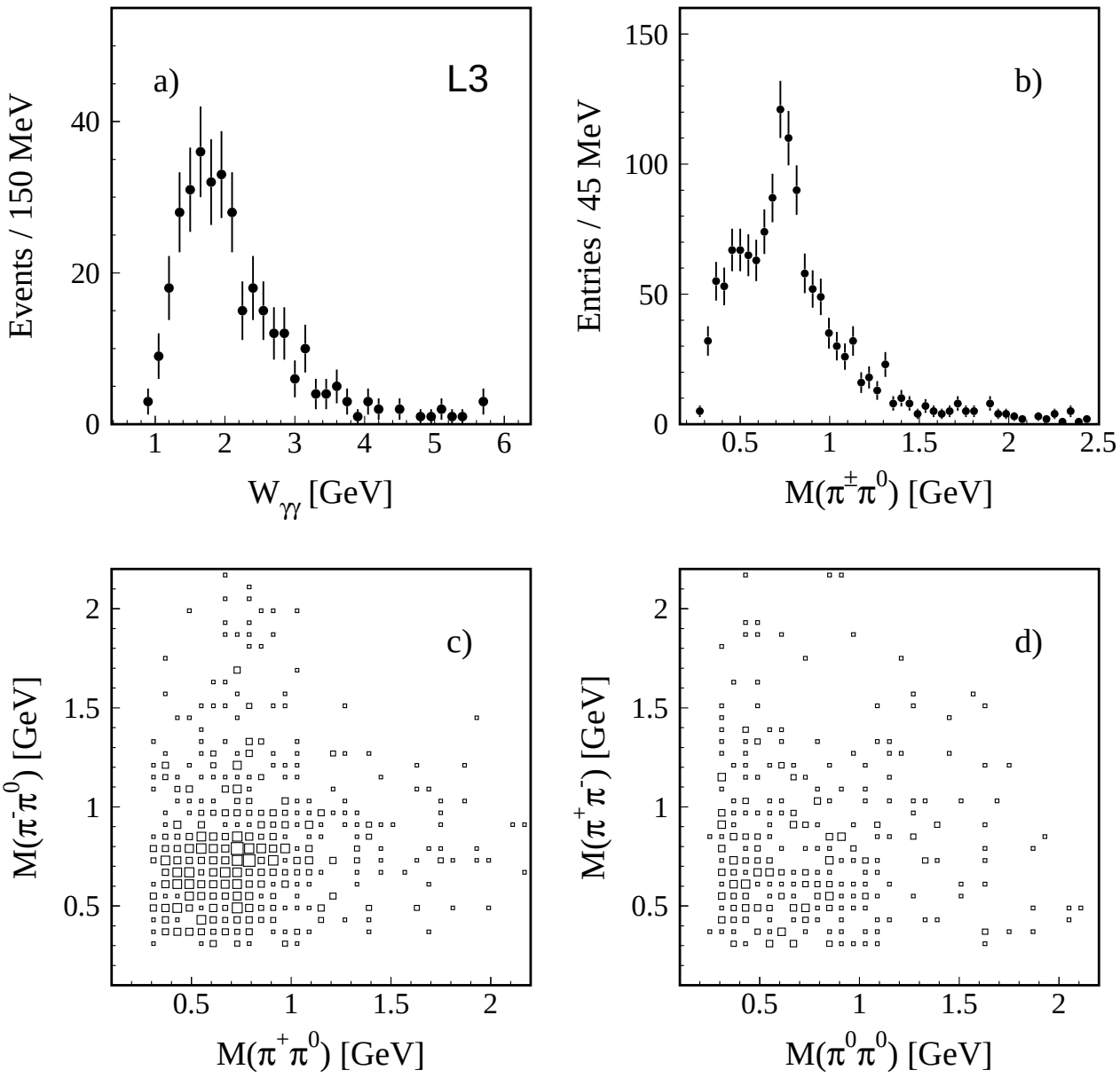

Figure 2: Effective mass distributions for the selected events: a) mass of the four-pion system, $W_{\gamma\gamma}$, b) mass of $\pi^{\pm}\pi^0$ combinations (four entries per event), c) correlation between the masses of the $\pi^-\pi^0$ and $\pi^+\pi^0$ pairs (two entries per event), d) correlation between the masses of the $\pi^+\pi^-$ and $\pi^0\pi^0$ pairs. The two-dimensional distributions have a bin width of 60×60 MeV^2, the size of the boxes is proportional to the number of entries and both plots have the same vertical scale.

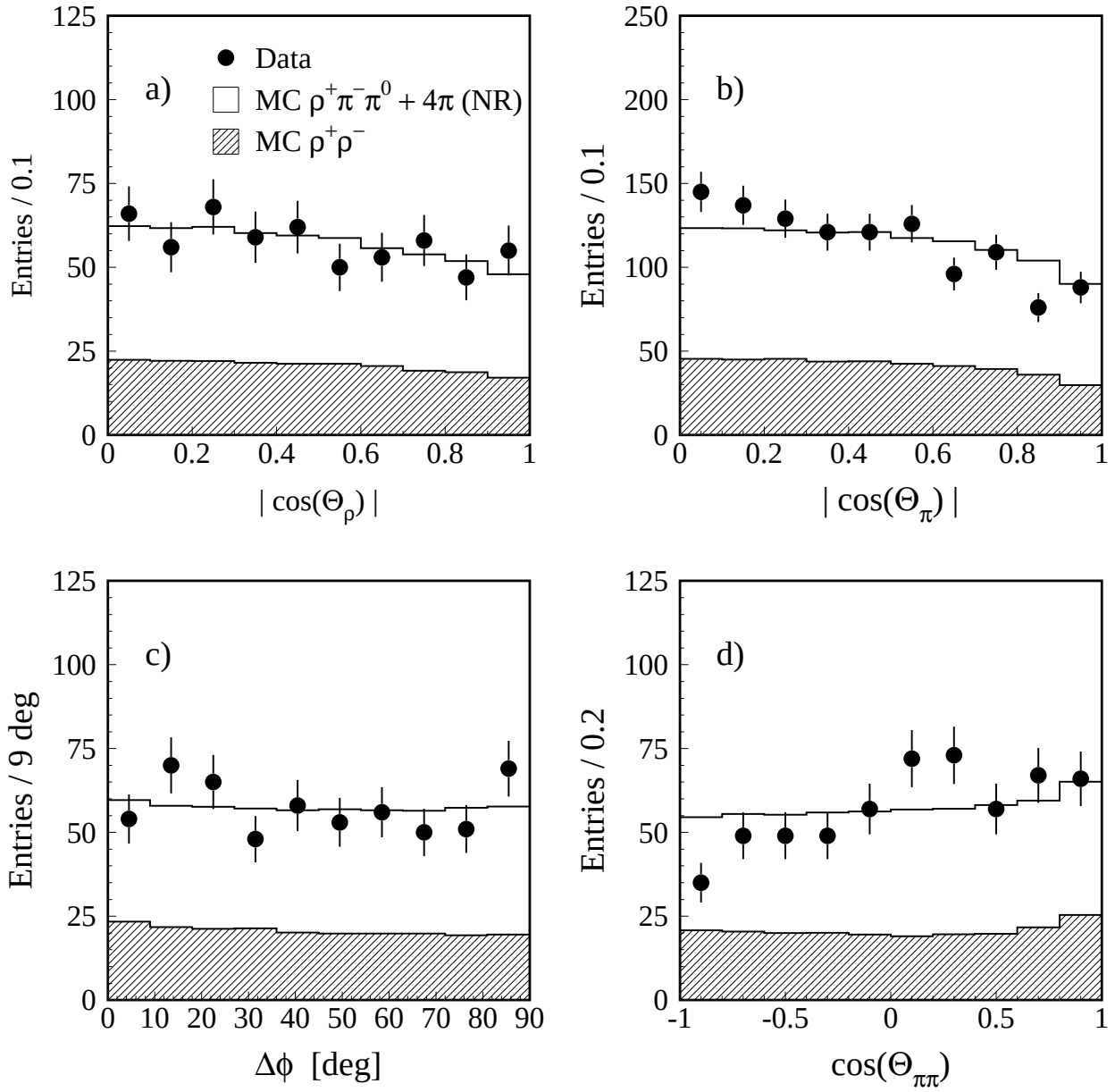

Figure 3: Comparison of data and Monte Carlo angular distributions: (a) $|\cos\Theta_\rho|$, the cosine of the polar angle of the $\rho^\pm$ with respect to the two-photon axis in the two-photon centre-of-mass system; (b) $|\cos\Theta_\pi|$, the cosine of the polar angle of the charged pion in its parent $\rho^\pm$ helicity-system; (c) $\Delta\phi$, the angle between the decay planes of the ρ^+ and ρ^- mesons in the two-photon centre-of-mass system; (d) $\cos\Theta_{\pi\pi}$, the cosine of the opening angle between the π^+ and π^- directions of flight, each one defined in its parent $\rho^\pm$ rest-system. There are two entries per event in (a), (c) and (d) and four entries per event in (b). The points represent the data, the hatched area shows the $\rho^+\rho^-$ component and the open area shows the sum of $\rho^\pm\pi^\mp\pi^0$ and $\pi^+\pi^-\pi^0\pi^0$ (non-resonant) components. The fraction of the different components are determined by the fit and the total normalisation is to the number of the events.

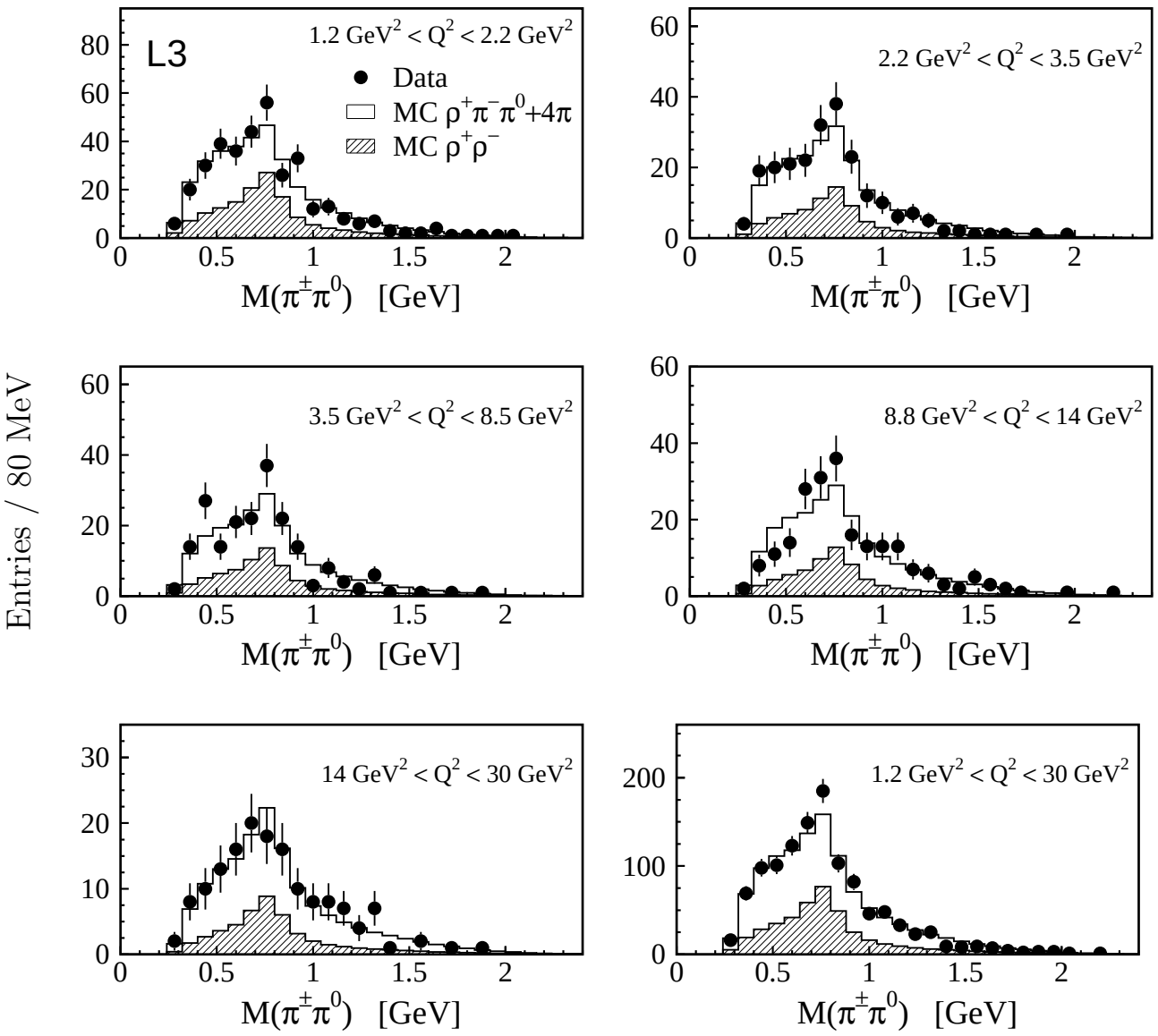

Figure 4: Effective mass distributions of $\pi^{\pm}\pi^0$ combinations (four entries per event) for events with 1.1 GeV $< W_{\gamma\gamma} <$ 3 GeV in the fitted Q^2 intervals. The points represent the data, the hatched area shows the $\rho^+\rho^-$ component and the open area shows the sum of $\rho^{\pm}\pi^{\mp}\pi^0$ and $\pi^+\pi^-\pi^0\pi^0$ (non-resonant) components. The fraction of the different components are determined by the fit and the total normalisation is to the number of the events. The plot for the entire Q^2 range, 1.2 GeV$^2 < Q^2 <$ 30 GeV^2, is the sum of the distributions of the five fitted Q^2 intervals.

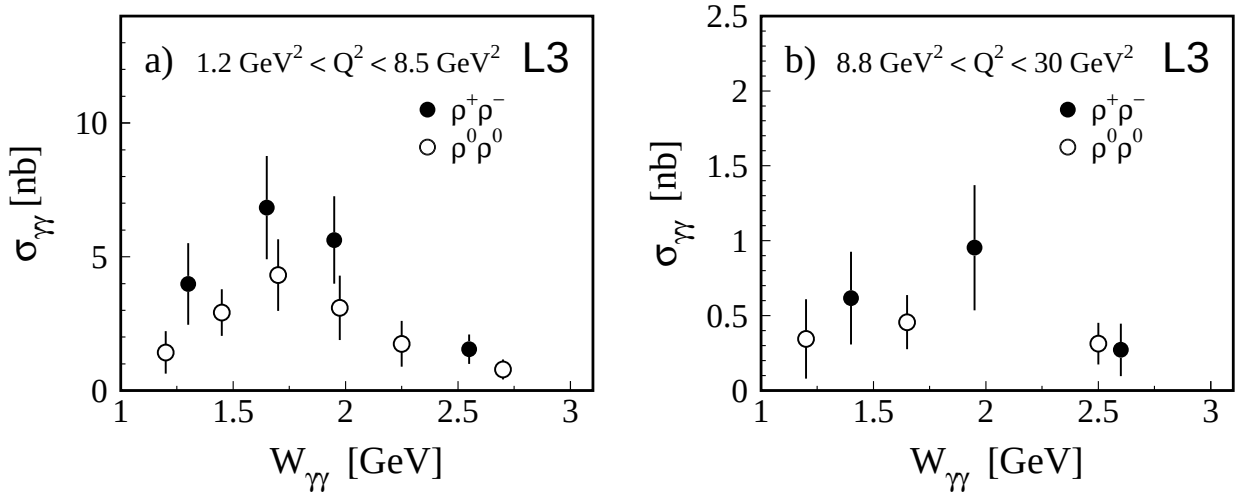

Figure 5: Cross section of the process $\gamma\gamma^* \to \rho\rho$ as function of $W_{\gamma\gamma}$, for a) 1.2 GeV^2 < Q^2 < 8.5 GeV^2 and b) 8.8 GeV^2 < Q^2 < 30 GeV^2. The full points show the results from this measurement, the open points show the results from the L3 measurement of $\rho^0\rho^0$ production [2], the bars show the statistical uncertainties.

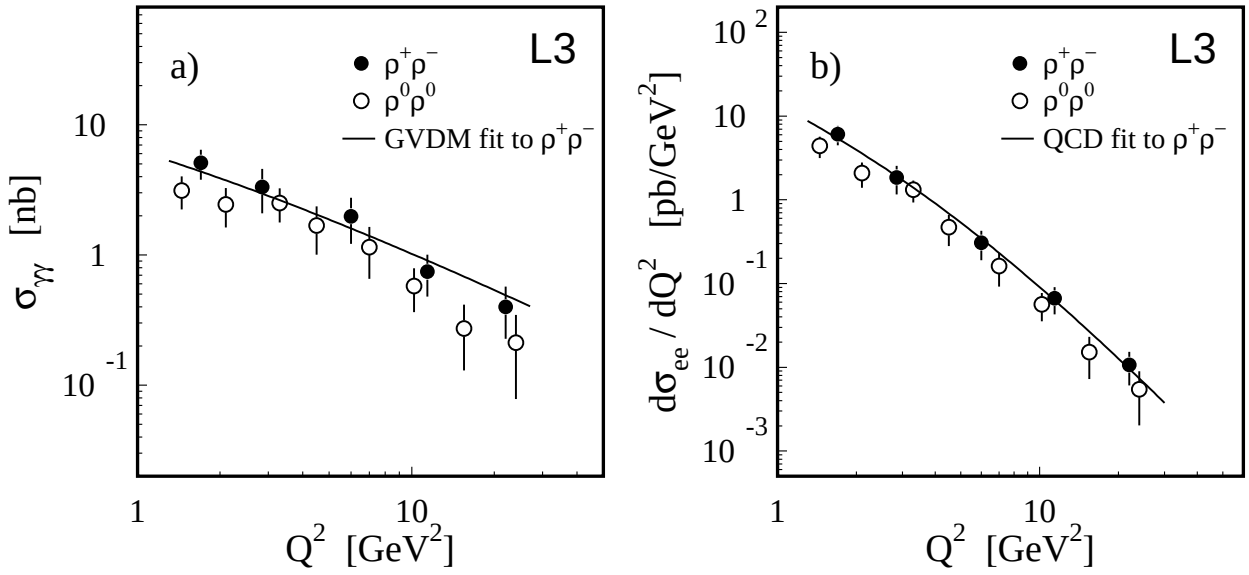

Figure 6: The $\rho\rho$ production cross section as a function of Q^2, for 1.1 GeV < $W_{\gamma\gamma}$ < 3 GeV: a) cross section of the process $\gamma\gamma^* \to \rho\rho$ and b) differential cross section of the process $e^+e^- \to e^+e^-\rho\rho$. The full points show the results from this measurement, the open points show the results from the L3 measurement of $\rho^0\rho^0$ production [2], the bars show the statistical uncertainties. The line in a) represents the result of a fit based on the generalised vector-meson dominance model [9]. The line in b) represents the result of a fit to a form expected from QCD calculations.